Journal of Non-Crystalline Solids 503–504 (2019) 36–43

Contents lists available at ScienceDirect

Journal of Non-Crystalline Solids

journal homepage: www.elsevier.com/locate/jnoncrysol

Synthesis of novel FeSiBPCCu alloys with high amorphous forming ability and good soft magnetic properties

Xingdu Fan[a,1], Tao Zhang[a,1], Mufeng Jiang[a,b], Weiming Yang[c], Baolong Shen[a,c,*]

[a] Jiangsu Key Laboratory for Advanced Metallic Materials, School of Materials Science and Engineering, Southeast University, Nanjing 211189, PR China
[b] Londerful New Material Technology Corp., Nantong 226233, PR China
[c] Institute of Massive Amorphous Metal Science, China University of Mining and Technology, Xuzhou 221116, PR China

ARTICLE INFO

Keywords:
Nanocrystalline alloy
Amorphous forming ability
Microstructure
Saturation magnetic flux density

ABSTRACT

Novel $Fe_{83.3}Si_4B_8P_{4-x}C_xCu_{0.7}$ (x = 0–4) alloys were developed with the aim of increasing amorphous forming ability (AFA) without deteriorating the soft magnetic properties. Microstructure analysis revealed that the substitution of C for P inhibited the precipitation of α-Fe phase during the quenching process hence increased the AFA. The critical thickness increased from 18 μm for the alloys with composition of x = 0 to 43 μm for x = 4, respectively, owing to the decrease in the melting entropy (ΔS_m), the approach of eutectic point and micro-alloying effect. Saturation magnetic flux density (B_s) increased obviously after proper annealing with increasing C substitution due to the increase in volume fraction of α-Fe nanocrystals, while excessive C content leaded larger coercivity (H_c) but improved the frequency and *DC* superposition performance. The $Fe_{83.3}Si_4B_8P_2C_2Cu_{0.7}$ nanocrystalline alloy was successfully synthesized with high B_s of 1.84 T, low H_c of 4.8 A/m and high effective permeability (μ_e) of 13,540. The combination of high B_s and high resistance to *DC* bias promises potential material in *DC* superposition application.

1. Introduction

Over the past three decades, nanocrystalline soft magnetic alloys of FeSiBNbCu, FeZrB(Cu) and FeCoZrBCu under the trade name of FINEMET, NANOPERM and HITPERM have been successively developed [1–3]. The research and application of nanocrystalline alloys [1–6] have greatly promoted the development of modern power electronic industry. However, with starting the problems of energy shortage and environmental pollution, more requirements are put forward on nanocrystalline alloys, and it becomes a noticeable topic to develop nanocrystalline alloys combined with high saturation magnetic flux density (B_s), low coercivity (H_c), low core loss, as well as low materials cost. The traditional nanocrystalline alloys cannot meet the above requirements anymore.

From 2009, nanocrystalline FeSiBPCu alloy (NANOMET) has attracted great attention due to its high B_s of > 1.8 T, low H_c of < 10 A/m and low material cost [7,8]. However, the relatively low amorphous forming ability (AFA), by which the ribbon thickness must be suppressed to 20 μm or less, constrains its application. Therefore, how to increase the AFA has become the crucial problem for NANOMET alloy.

It has been reported that flux melting is an effective way to improve the AFA [9,10]. The fluxing purification by B_2O_3 and CaO has been proved feasible to increase the AFA in high B_s FeSiBPC amorphous alloy because it can suppress the surface crystallization and alleviate the effect of detrimental impurity such as oxide and sulfide [11]. But the complex fluxing process increases the manufacturing cost. Recently, it is found that a proper amount of Co substitution for Fe in NANOMET-type alloys is effective to increase the AFA without losing high B_s because the addition of Co decreases the liquidus temperature which facilitates the amorphous phase formation [12,13]. However, noble metal elements such as Co compared to others present in the alloy detract the commercialization. Recent researches suggest that minor C addition is effective to obtain good soft magnetic properties (SMP) in thicker ribbons [14–17]. The enhancement of AFA by C addition is owing to the small size of metalloid atom which disrupts the short-range order, the formation of competition complex phases which impedes the devitrification as well as the approach of deep eutectic point. Nevertheless, the above researches are only based on a small amount of C addition with < 1 at.%. Meanwhile, it is worth mentioning that P plays a crucial role on AFA and SMP of NANOMET alloys as there are previous reports

* Corresponding author at: Jiangsu Key Laboratory for Advanced Metallic Materials, School of Materials Science and Engineering, Southeast University, Nanjing 211189, PR China.
E-mail address: blshen@seu.edu.cn (B. Shen).
[1] Authors contributed equally to this work.

https://doi.org/10.1016/j.jnoncrysol.2018.09.021
Received 18 July 2018; Received in revised form 7 September 2018; Accepted 13 September 2018
Available online 20 September 2018

revealing that the Cu_3P like clusters are easily formed due to the strong attractive interaction between P and Cu atoms, which possibly act as nucleation sites for α-Fe phase in the as-quenched state and consequently lead to the formation of the hetero-amorphous structure [18,19]. Therefore, with the aim of synthesizing a novel NANOMET-type alloy with higher AFA, good SMP as well as low cost, we developed the $Fe_{83.3}Si_4B_8P_{4-x}C_xCu_{0.7}$ (x = 0, 1, 2, 3, 4) alloys. The influence of C substitution for P on amorphous forming ability, crystallization behavior, microstructure and soft magnetic properties in FeSiBPCCu alloys was investigated.

2. Experimental procedures

Alloy ingots with nominal compositions of $Fe_{83.3}Si_4B_8P_{4-x}C_xCu_{0.7}$ (x = 0, 1, 2, 3, 4, denoted as C_0 to C_4, respectively) were prepared by induction melting the mixtures of Fe (99.99 mass%), Si (99.99 mass%), B (99.5 mass%), Cu (99.99 mass%) and pre-alloyed Fe—P and Fe—C alloy under an argon atmosphere. The alloy ingots were re-melted in a quartz tube with nozzle in the bottom under an argon atmosphere and then sprayed into a rapidly rotating copper wheel under a pressure of 0.02 MPa to obtain amorphous ribbons. The nozzle size is 0.5 mm in diameter and the distance between nozzle and copper wheel is 0.3 mm. Ribbon thickness was controlled by changing the linear wheel speed in a range of 20–50 m/s. The width and thickness were 1 mm and 16–50 μm, respectively. Thermal stability associated with crystallization temperature (T_x) and melting temperature (T_m) of melt-spun alloys was examined by differential scanning calorimetry (DSC) at a heating rate of 0.67 °C/s. The liquidus temperature (T_l) was measured with DSC by cooling the molten alloy samples at a cooling rate of 0.067 °C/s. The melting enthalpy (ΔH_m) was determined by the area of the melting peak and, accordingly the melting entropy (ΔS_m) was calculated using the definition of $\Delta S_m = \Delta H_m/T_m$. Melt-spun ribbons were isothermally annealed to develop nanocrystalline alloys. The annealing was carried out by keeping the ribbons in a quartz tube under vacuum atmosphere (10^{-3} Pa), and then pushing the quartz tube into a tubular furnace preheated to annealing temperature (410–530 °C) for 3 min followed by water quenching cooling. Microstructures were identified by X-ray diffraction (XRD) with Cu $K\alpha_1$ radiation and transmission electron microscopy (TEM). TEM samples were prepared by ion milling method (Gatan Inc., PIPS-M691) under liquid nitrogen cooling condition. The volume fraction (V_{cry}) of α-Fe nanocrystals is calculated by equation $V_{cry} = I_{cry}/(I_{cry} + I_{amo})$ where I_{cry} and I_{amo} stand for the integral intensities of diffraction peaks for crystallization phase and amorphous phase, respectively [20]. The values of V_{cry} can be calculated using the Jade 5.0 software by peak fitting. B_s and H_c under a maximum applied field of 800 kA/m and 1 kA/m were measured by a vibrating sample magnetometer (VSM) and a *DC* B—H loop tracer, respectively. Permeability was measured with an impedance analyzer under a field of 1 A/m. Resistance to *DC* bias was identified by an impedance analyzer under applied *DC* field from 1 to 120 A/m. Measurement errors (such as B_s, H_c, etc.) were determined by averaging the measured values of 5 specimens and calculation errors (such as ΔS_m, V_{cry}, etc.) were determined by multiple calculations.

3. Results and discussion

Fig. 1 (a) shows the XRD patterns of free surface of $Fe_{83.3}Si_4B_8P_{4-x}C_xCu_{0.7}$ melt-spun ribbons with 20–21 μm in thickness. It can be seen that there is a sharp crystallization peak at $2\theta = 65°$ existing for $Fe_{83.3}Si_4B_8P_4Cu_{0.7}$ alloy which is related to the (200)-reflection of the crystalline α-Fe phase. However, with increasing C addition, the crystallization peak disappeared and all samples exhibit halo patterns, indicating the formation of amorphous structure. Since surface crystallization behavior is common in high Fe content alloys [21–23], further analysis is taken for the C_0 alloy. Fig. 1 (b) presents the XRD patterns of $Fe_{83.3}Si_4B_8P_4Cu_{0.7}$ alloy in different conditions. The wheel side of

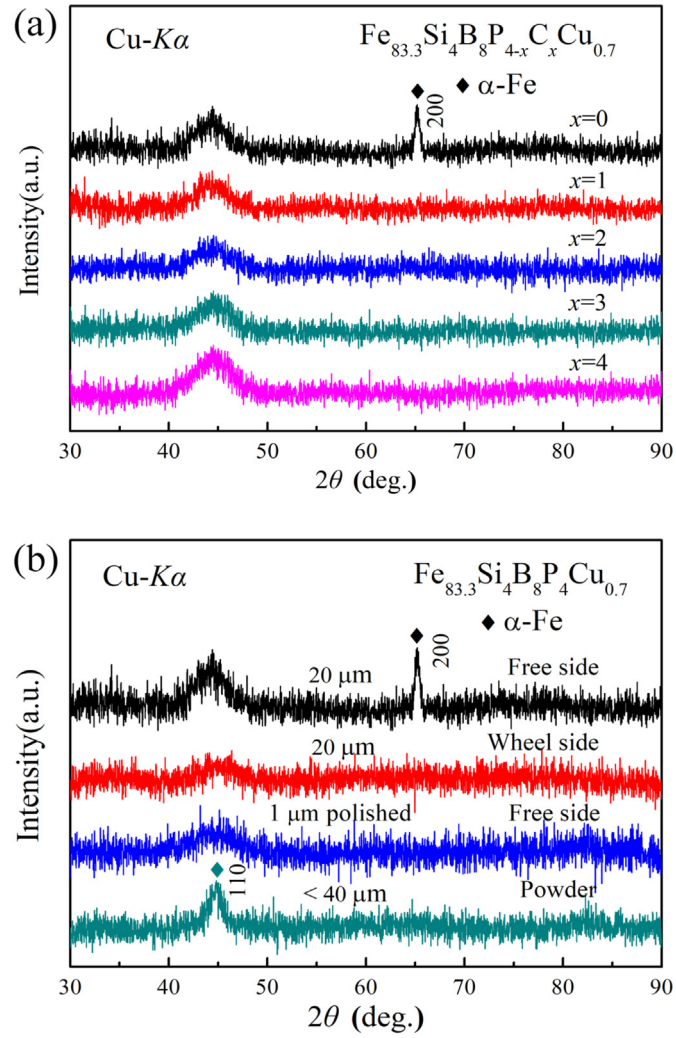

Fig. 1. XRD patterns of (a) free surface of $Fe_{83.3}Si_4B_8P_{4-x}C_xCu_{0.7}$ melt-spun ribbons and (b) $Fe_{83.3}Si_4B_8P_4Cu_{0.7}$ melt-spun ribbons in different conditions.

ribbon sample shows broad peak without appreciable crystallization peaks, which confirms the crystallization only appears on the free side. The in-plane crystalline texture is induced only on the free surface area during quenching, as can be proven by mechanical polishing. As shown in Fig. 1 (b), the ribbon sample polished by 1 μm shows amorphous feature indicating the surface crystallization layer is < 1 μm. It has been revealed that the (200) texture is oriented parallel to the ribbon surface, but there is no preferred orientation along the long ribbon axis [22,23]. In order to confirm this phenomenon, the $Fe_{83.3}Si_4B_8P_4Cu_{0.7}$ powder ground manually in alcohol from the melt-spun ribbon was characterized. It is found that the crystallization peak at $2\theta = 65°$ disappears and only a small diffraction peak appears at about $2\theta = 44.5°$ for the powders with particle sizes < 40 μm. The result reveals that the (200) texture disappeared when the ribbon is ground into powder, which is well consistent with previous result [22].

Single roller melt-spinning method was used to evaluate the AFA. Ribbon thickness was controlled by changing the wheel speed. The critical thickness and wheel speed were selected as the characteristics of AFA. Fig. 2 shows the XRD patterns of free surface of $Fe_{83.3}Si_4B_8P_{4-x}C_xCu_{0.7}$ (x = 0, 2, 4) melt-spun ribbons with different thickness. For C_0 alloy, only 16–18 μm-thick amorphous ribbon can be prepared with a high wheel speed of 50 m/s. The C-containing alloys exhibit higher AFA and can be made into single amorphous phase at a lower speed (25–35 m/s). Increasing the ribbon thickness to above 20 μm for C_0 and 39 μm for C_2 ribbons results in the appearance of a sharp crystallization

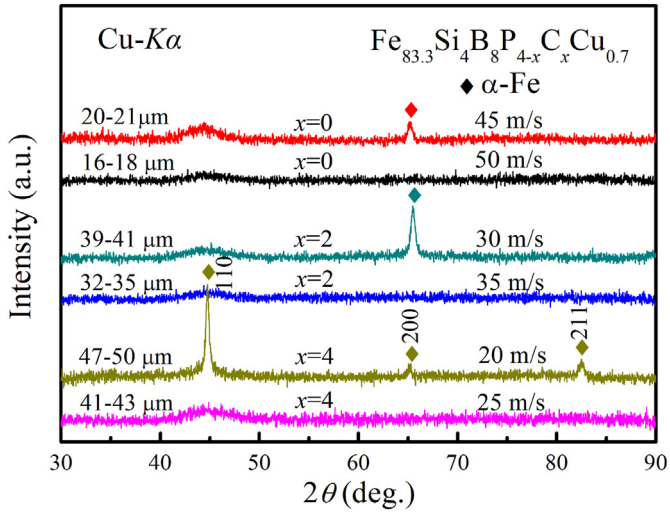

Fig. 2. XRD patterns of free surface of $Fe_{83.3}Si_4B_8P_{4-x}C_xCu_{0.7}$ (x = 0, 2, 4) melt-spun ribbons with different thickness.

peak at 2θ = 65°, which is associated with the surface crystallization. However, the 47–50 μm-thick C_4 sample shows the Bragg peaks associated with three characteristic diffraction peaks of α-Fe, indicating the precipitation of nanocrystalline α-Fe phase.

Fig. 3 summarizes the amorphous forming ability characterized by critical thickness. The AFA of $Fe_{83.3}Si_4B_8P_4Cu_{0.7}$ alloy is improved significantly by C substitution and the critical thickness increases from 18 μm for C_0 alloy to 43 μm for C_4 alloy. It is noted that the AFA of C_4 alloy is higher than that of NANOMET-type alloys with 34 μm in critical thickness [15]. The result seems to be inconsistent with previous reports which indicate that C addition can effectively increase the AFA, but the optimal C content is ≤ 0.3 at.% and the critical thickness is limited to 25 μm or less [16,17]. The present result shows that even > 2 at.% C additions are beneficial to the formation of amorphous phase. The primary phase is determined as α-Fe (200) phase for the C free and minor C-containing alloys, however it changes into α-Fe phases with different orientation by complete C substitution. The formation of crystalline α-Fe phase with different textures may be beneficial for the AFA due to the competing effect.

Thermodynamic properties of melt-spun ribbons were investigated for further understanding the AFA. The ribbons used for the following measurement are 20–21 μm in thickness. Fig. 4 (a) shows the DSC

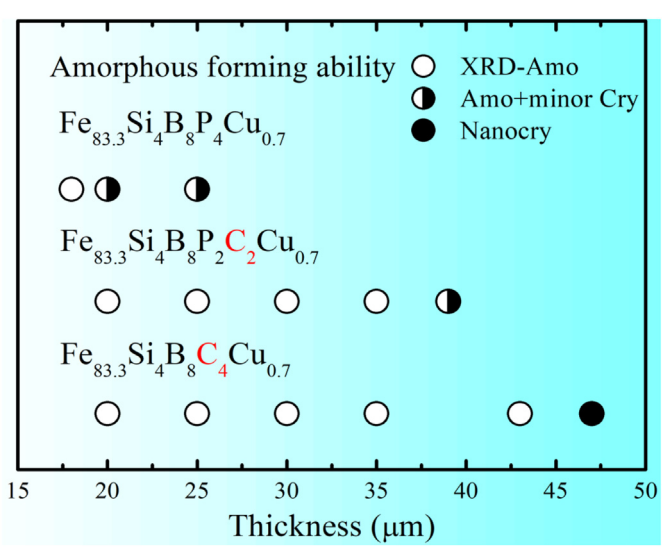

Fig. 3. Amorphous forming ability of $Fe_{83.3}Si_4B_8P_{4-x}C_xCu_{0.7}$ alloys (x = 0, 2, 4).

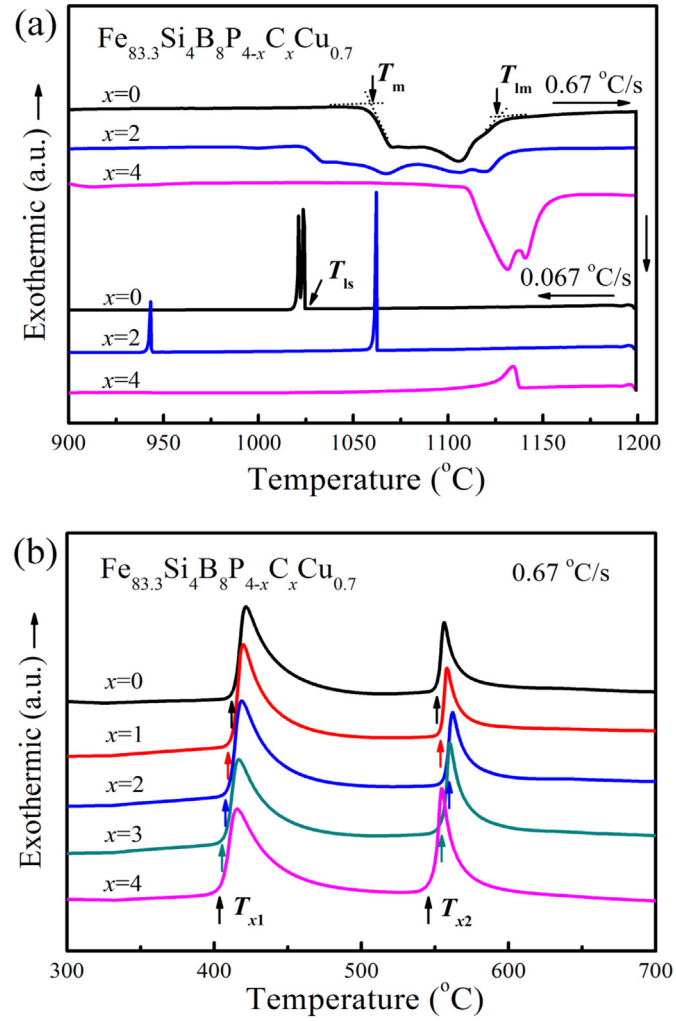

Fig. 4. DSC curves of (a) the melting and solidification processes for $Fe_{83.3}Si_4B_8P_{4-x}C_xCu_{0.7}$ (x = 0, 2, 4) alloys and (b) the crystallization process for $Fe_{83.3}Si_4B_8P_{4-x}C_xCu_{0.7}$ alloys.

curves of the melting and solidification processes for $Fe_{83.3}Si_4B_8P_{4-x}C_xCu_{0.7}$ (x = 0, 2, 4) alloys. The onset and offset temperatures of the melting endothermic event are designated by T_m and T_{lm}. The onset temperature of the solidification exothermic event is designated by T_{ls}. The thermal parameters are listed in Table 1. With 2 at.% C addition, the melting temperature interval between T_m and T_{1m} increases from 70 to 105 °C, combined with the increase in T_{ls}, which means poor AFA. However, the ΔH_m decreases clearly, indicating the lower binding energy of the crystalline phases. Meanwhile, the calculated ΔS_m (3.56 J/mol-K) for C_2 alloy is lower than that of C_0 alloy, which favors the formation of amorphous, as it has been experimentally evidenced that alloys of higher AFA generally have lower ΔS_m [24–26]. ΔS_m has long been recognized as a crucial thermodynamic quantity in determining kinetic behaviors of materials. In addition to decreasing thermodynamic driving forces for crystallization in a liquid-solid transition, low ΔS_m also reduces crystal growth rate and interfacial tension, steepens the profiles of liquidus lines in equilibrium phase diagrams which have an advantage in obtaining deep eutectics therefore favors the glass formation [25,26]. With further increasing C content to 4 at.%, the melting temperature interval decreases obviously from 105 to 50 °C, implying that the composition of the alloy lies in the vicinity of a eutectic point with further increasing C addition. Although the C_4 alloy exhibits a higher T_{ls} due to the substitution of C element with high melting point, which may lead to the increase in eutectic temperature,

Table 1
Thermal properties, amorphous forming ability, soft magnetic properties and microstructure parameters of $Fe_{83.3}Si_4B_8P_{4-x}C_xCu_{0.7}$ alloys annealed at 450 °C for 3 min.

Alloys	Thermal properties					AFA			Magnetic properties				Microstructure parameters		
	T_{x1} (°C)	T_{x2} (°C)	T_m (°C)	T_{lm} (°C)	ΔS_m (J/mol-K)	E_p (kJ/mol)	V_c (m/s)	T (μm)	B_s (T)	H_c (A/m)	μ_e (1 kHz)	μ_{120}/μ_e (%)	D (nm)	V_{cry} (%)	N_d (m^{-3})
$Fe_{83.3}Si_4B_8P_4Cu_{0.7}$	414	552	1058	1128	4.13 ± 0.05	255 ± 5	50	18 ± 1	1.69 ± 0.01	4.3 ± 0.3	17,380 ± 500	44.9 ± 2.8	14 ± 0.5	30.5 ± 2.0	1.1×10^{23}
$Fe_{83.3}Si_4B_8P_3C_1Cu_{0.7}$	413	554	1021	1132	3.39 ± 0.05	–	–	–	1.82 ± 0.01	5.3 ± 0.4	11,850 ± 420	55.5 ± 3.7	19 ± 0.5	50.4 ± 2.1	–
$Fe_{83.3}Si_4B_8P_2C_2Cu_{0.7}$	410	558	1025	1130	3.56 ± 0.04	269 ± 5	35	35 ± 1	1.84 ± 0.01	4.8 ± 0.3	13,540 ± 450	53.5 ± 3.7	22 ± 0.5	55.6 ± 2.2	5.2×10^{22}
$Fe_{83.3}Si_4B_8P_1C_3Cu_{0.7}$	408	556	1025	1134	3.09 ± 0.06	–	–	–	1.85 ± 0.01	22.0 ± 2.1	9670 ± 340	72.6 ± 4.9	28 ± 0.6	58.7 ± 2.2	–
$Fe_{83.3}Si_4B_8C_4Cu_{0.7}$	406	550	1110	1160	3.46 ± 0.05	230 ± 5	25	43 ± 1	1.85 ± 0.01	23.3 ± 2.2	6780 ± 240	71.1 ± 4.9	34 ± 0.8	60.6 ± 2.2	1.5×10^{22}

the ΔS_m is only 3.46 J/mol-K and the alloy shows only one solidification exothermic peak, further implying the approach of a eutectic point that exhibits a higher AFA. In addition, the C atom with small atomic radius can occupy interstitial spaces among the major constituent atoms, leading to the increase in packing density of the liquids. The strong atomic bonding between Fe and C due to the large negative heat of mixing (Fe-C: −50 kJ/mol) [27] can enhance the short-range order of amorphous-forming liquids, which also impedes the devitrification of primary α-Fe phase [28]. Consequently, taking a combination of the lower melting entropy, closer to the eutectic point and micro-alloying effect into consideration, it is concluded that the C_4 alloy possesses a higher AFA with 43 μm in critical thickness.

In order to investigate the magnetic properties, $Fe_{83.3}Si_4B_8P_{4-x}C_xCu_{0.7}$ alloy ribbons were annealed to develop nanocrystalline alloys. The crystallization behavior was first measured to determine the annealing temperature (T_a). Fig. 4 (b) shows the DSC curves of $Fe_{83.3}Si_4B_8P_{4-x}C_xCu_{0.7}$ melt-spun ribbons showing the crystallization process. There are two exothermic peaks for the alloys indicating the crystallization process includes two stages. According to former research results, the first onset crystallization temperature (T_{x1}) is associated with the primary crystallization of α-Fe phase while the second one (T_{x2}) corresponds to formation of FeBP compounds [29]. The T_{x1} shows a slight decrease with C increasing, which indicates that the C substitution for P favors the precipitation of initial α-Fe phase. Although the temperature difference between T_{x1} and T_{x2} shows no obvious change with the increase in C addition, the large temperature intervals over 138–148 °C are beneficial for the formation of α-Fe phase without nonferromagnetic phase precipitation, which is advantageous for achieving good SMP.

Fig. 5 shows the XRD patterns of $Fe_{83.3}Si_4B_8P_{4-x}C_xCu_{0.7}$ alloys annealed at 450 °C for 3 min. As a result, single α-Fe phase is precipitated obviously from amorphous matrix for the annealed alloys. The intensity of diffraction peak corresponding to the (110) α-Fe phase increases gradually with the increasing C addition, which means higher crystallization. The volume fraction (V_{cry}) of α-Fe nanocrystals is from 30.5% to 60.6% with the increase in x from 0 to 4, while the average grain size (D) estimated by Scherrer's equation according to the (110) diffraction peak is 15, 19, 21, 28 and 32 nm, respectively, indicating that C substitution for P simultaneously enlarges the V_{cry} and D.

The dependence of H_c on T_a for $Fe_{83.3}Si_4B_8P_{4-x}C_xCu_{0.7}$ alloys is shown in Fig. 6. Here AQ stands for H_c of as-quenched alloys. According to the result, H_c first decreases at T_a = 410 °C. This decrease is mainly caused by initial stress relief. Then for the alloys with composition of x = 0–2, H_c first increases slightly at T_a = 430 °C due to the low

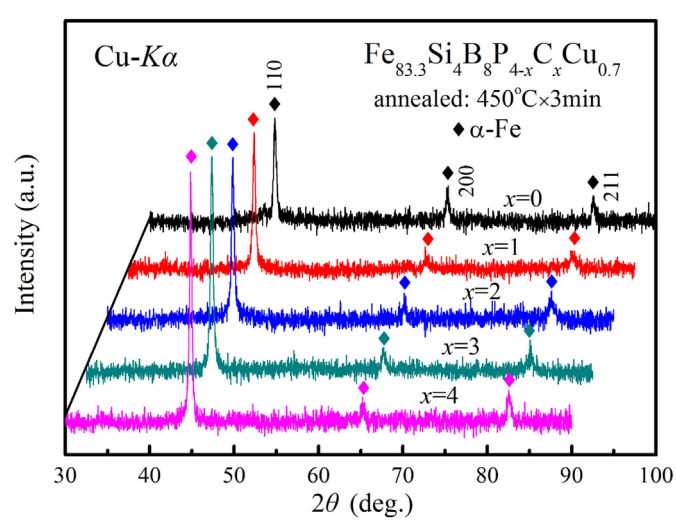

Fig. 5. XRD patterns of $Fe_{83.3}Si_4B_8P_{4-x}C_xCu_{0.7}$ alloys annealed at 450 °C for 3 min.

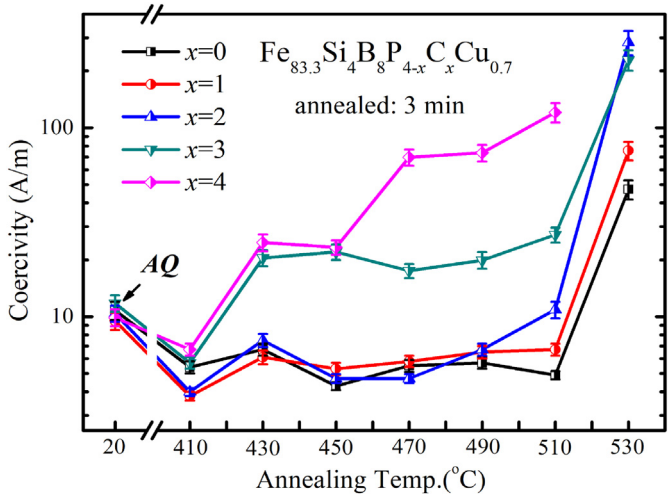

Fig. 6. The dependence of coercivity (H_c) on annealing temperature (T_a) for $Fe_{83.3}Si_4B_8P_{4-x}C_xCu_{0.7}$ alloys.

nucleation rate at low T_a. With further increased T_a, H_c decreases again and keeps at a low value in a wide T_a range between 450 and 510 °C, implying good thermal stability. When T_a is increased to 530 °C, H_c increases dramatically due to the growth of α-Fe nanocrystals and/or the precipitation of nonferromagnetic phases as 530 °C is very close to the second crystallization temperature. The H_c for the C_3 alloy shows a similar variation trend, the difference is that it keeps at a larger value above 17.5 A/m in the same T_a range. While for the C_4 alloy, H_c has been increased dramatically at 470 °C and cannot be detected by B–H loop tracer at 530 °C as the hysteresis loop exhibits paramagnetic characteristic. According to the results, the optimum T_a is fixed as 450 °C.

The hysteresis loops of $Fe_{83.3}Si_4B_8P_{4-x}C_xCu_{0.7}$ alloys annealed at 450 °C for 3 min were then measured as shown in Fig. 7. Accordingly, the B_s of annealed alloys increases obviously from 1.69 to 1.82 T with 1 at.% C substitution and continue to increase with further increasing C content as shown in the upper-left illustration. The increase in B_s is caused by the increasing V_{cry} of α-Fe nanocrystals as the value of B_s is dependent on the magnetization in crystalline and amorphous phases. The B_s of the former is much larger than the latter, therefore the higher the V_{cry}, the superior the B_s [30]. From the inset hysteresis curves detected from *DC* B–H loop tracer, it is known that the alloys with proper

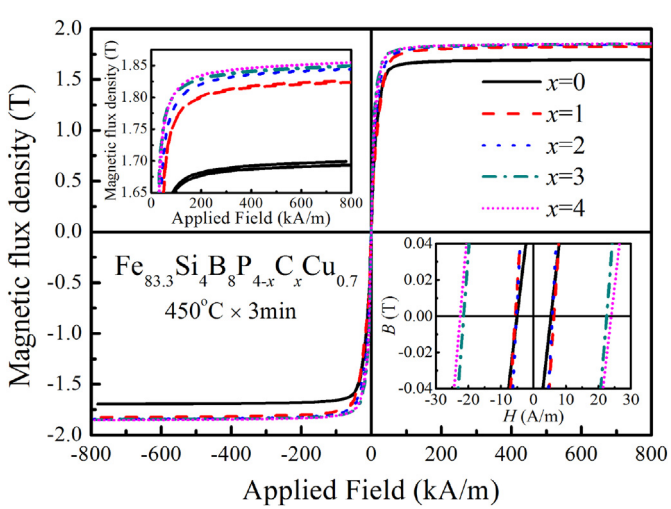

Fig. 7. Hysteresis loops of $Fe_{83.3}Si_4B_8P_{4-x}C_xCu_{0.7}$ alloys annealed at 450 °C for 3 min. The inset is a partial enlargement of that of approaching saturation and hysteresis curves measured by *DC* B–H loop tracer at applied field of 1 kA/m.

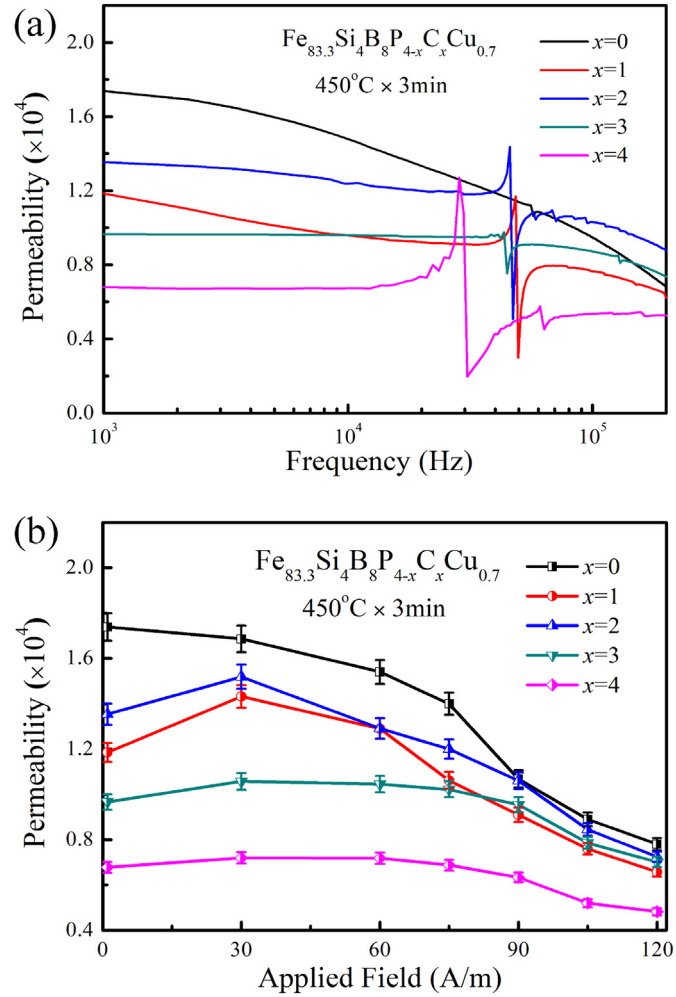

Fig. 8. The dependence of permeability on (a) frequency and (b) applied *DC* field for $Fe_{83.3}Si_4B_8P_{4-x}C_xCu_{0.7}$ alloys annealed at 450 °C for 3 min.

C addition exhibit low H_c of < 5 A/m. It is noted that the annealed C-containing alloys exhibit larger slopes which indicates the higher permeability at an applied field of 1 kA/m.

Considering the relative permeability (μ) under high frequency and applied *DC* field is an important parameter in application for nanocrystalline alloys [31,32], the dependence of permeability on frequency for $Fe_{83.3}Si_4B_8P_{4-x}C_xCu_{0.7}$ alloys annealed at 450 °C for 3 min was measured. As shown in Fig. 8 (a), the effective permeability (μ_e) shows a decreasing tendency with increasing C substitution. Although the annealed C_0 alloy possesses the largest μ_e of 17,380, the μ decreases dramatically towards frequency, from which indicating the frequency characteristic is inferior but can be improved by C addition. For the alloy with composition of $x \geq 2$, the μ almost remains unchanged in the wide frequency range of 1–200 kHz. Fig. 8 (b) shows the dependence of permeability on applied *DC* field for $Fe_{83.3}Si_4B_8P_{4-x}C_xCu_{0.7}$ alloys annealed at 450 °C for 3 min. It can be seen that the μ decreases gradually towards the density of applied field for the C_0 alloy. With C substitution, there is a slightly increase for μ and the maximum value is reached at 30 A/m, which is quite consistent with the previous researches [32]. For the C_3 and C_4 alloys, the μ exhibits almost no decrease until the amplitude applied field is above 90 A/m. The value of μ under an applied *DC* field of 120 A/m is 7020 for C_3 and 4820 for C_4 alloy, which is 72.6% and 71.1% of μ_e, respectively, indicating high resistance to *DC* bias.

Since soft magnetic properties are significantly associated with microstructure, further analysis of microstructure was studied by TEM.

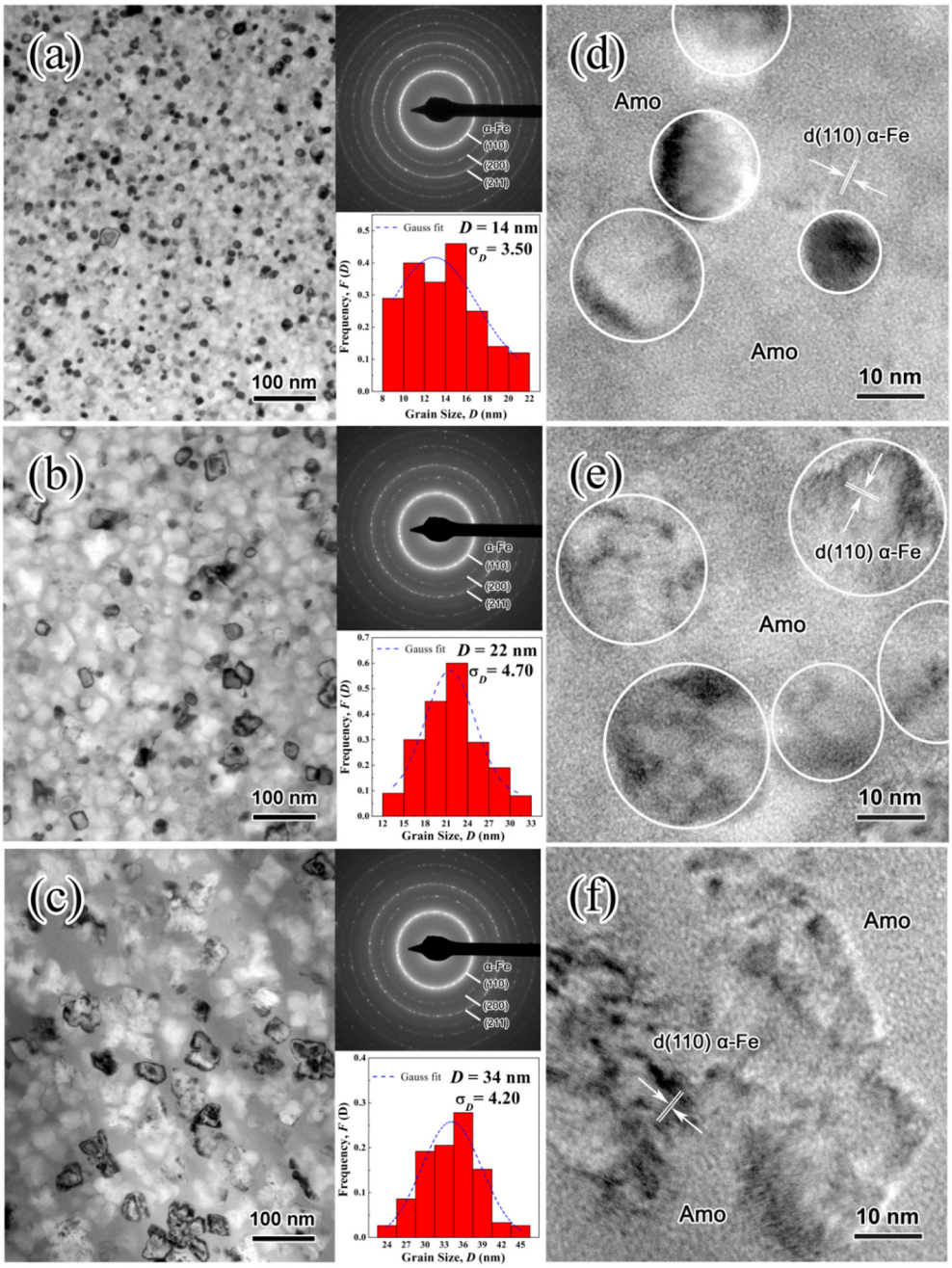

Fig. 9. The bright-field TEM images, selected area electron diffraction (SAED) patterns, grain size distributions and corresponding high resolution-TEM (HRTEM) images of $Fe_{83.3}Si_4B_8P_{4-x}C_xCu_{0.7}$ alloys annealed at 450 °C for 3 min with (a) and (d): $x = 0$; (b) and (e): $x = 2$; (c) and (e): $x = 4$, respectively. The blue dotted lines show Gauss fit. (For interpretation of the references to colour in this figure legend, the reader is referred to the web version of this article.)

Fig. 9 presents the TEM images of $Fe_{83.3}Si_4B_8P_{4-x}C_xCu_{0.7}$ alloys annealed at 450 °C for 3 min with composition of $x = 0$, 2 and 4, respectively. The bright-field TEM images and SAED patterns (*see* Fig. 9 (a)-(c)) reveal that α-Fe nanocrystalline grains precipitate from amorphous matrix after annealing but the grain size and distribution are quite different. For the annealed C_0 alloy, the precipitated α-Fe grains are relatively small but more uniform. Statistic result reveals that the grain distributes mainly from 8 to 18 nm with 14 nm in average. The number density (N_d) of α-Fe grain is around $1.1 \times 10^{23}\,m^{-3}$, which is consistent with previously reported NANOMET alloy [33]. Annealed C_2 alloy also exhibits a uniform nanostructure but the grain size is obviously larger compared with the C_0 alloy. As for the C_4 alloy, the average D is as large as 34 nm and N_d is decreased from $5.2 \times 10^{22}\,m^{-3}$ to $1.5 \times 10^{22}\,m^{-3}$. The decrease in N_d is resulted from the decreasing P content, as there have been reports revealing that the coordination of P and Cu atom can provide more heterogeneous nucleation sites to promote the nucleation of α-Fe primary crystals [19,34,35]. Therefore, the alloy with more P-content leads to a higher N_d which greatly lowers the grain size. It has also been reported that P in NANOMET alloy contributes to stabilizing residual amorphous phase hence inhibits the grain growth [36,37]. What is more, the mean square deviation (σ_D) for C_0 alloy is only 3.50, which is smaller than that of C-containing sample ($\sigma_D \geq 4.20$), further reflecting a more uniform nanostructure.

The HRTEM observation (*see* Fig. 9 (d)-(f)) reveals that the structure and grain shape of α-Fe nanocrystals have certain difference. There exists a large amount of residual amorphous phase for annealed C_0 alloy. However, the increasing C substitution clearly lowers the N_d, resulting in the growth of α-Fe grain thus increasing the V_{cry}. The result

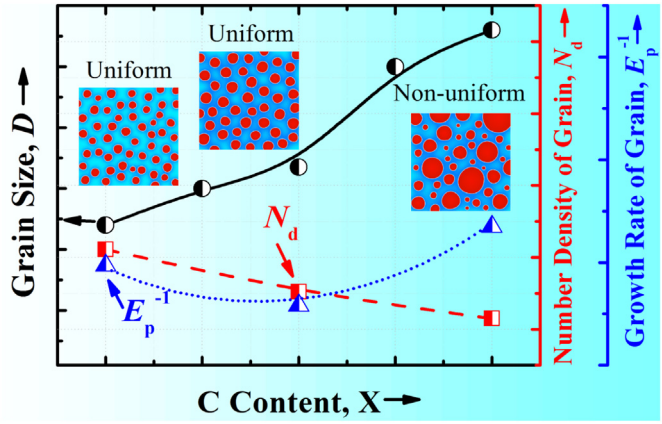

Fig. 10. Microstructure schematics showing the variation trend of grain size (D), number density (N_d) and growth rate (E_p^{-1}) of α-Fe grain dependent on C content for FeSiBPCCu nanocrystalline alloys.

is quite consistent with the XRD measurement. Meanwhile, the grain profiles for annealed C_0 and C_2 alloys are circular while the C_4 alloy appears elongated, indicating the existence of orientation growth of α-Fe crystals and large magneto-crystalline anisotropy.

Since crystallization is a solid-state phase transformation controlled by nucleation and growth kinetics, it is important to further understand the reason why proper C substitution for P is beneficial for the formation of nanocrystalline alloys with uniform nanostructure. The crystallization kinetics was studied by using the Kissinger method [38]. The activation energy (E_p) deduced from the first peak temperatures corresponding to the growth of α-Fe grain is calculated as listed in Table 1, the C_2 alloy exhibits the largest E_p of 269 kJ/mol, implying a low growth rate of α-Fe grain. With further increased C addition, the E_p decreases to 230 kJ/mol, indicating the easy growing of α-Fe grain.

Fig. 10 illustrates the microstructure schematics showing the variation trend of D, N_d and growth rate (E_p^{-1}) of α-Fe grain dependent on C content for FeSiBPCCu nanocrystalline alloys. As mentioned above, the high N_d of ~1.1×10^{23} and relatively low E_p^{-1} make the C free alloy possess ultrafine nanostructure with uniform distribution of α-Fe phase. As for the alloy with minor C addition, although the N_d is less than that of C free alloy, the larger E_p indicates the growth of α-Fe grain is effectively inhibited. The competition between relatively low nucleation density and low growth rate of α-Fe grain also results in a fine nanostructure. However, the excessive C addition not only lowers the N_d but also degrades the thermal stability, which leads to the rapid and non-uniform growth of α-Fe grains, thereby deteriorating the SMP.

Table 1 summarizes the thermal properties, AFA, SMP and microstructure parameters of $Fe_{83.3}Si_4B_8P_{4-x}C_xCu_{0.7}$ alloys annealed at 450 °C for 3 min. The $Fe_{83.3}Si_4B_8P_2C_2Cu_{0.7}$ nanocrystalline alloy simultaneously possesses high B_s of 1.84 T and low H_c of 4.8 A/m. Though H_c is slightly larger than C_0 alloy, the obviously higher V_{cry} with ultrafine nanostructures and homogenous distribution lead to the strengthening of exchange-coupling interaction, which not only effectively superiors the B_s, but also reduces effective magneto-crystalline anisotropy $< K >$ thereby decreasing the H_c as it has been proved by the random anisotropy model which suggests that H_c is directly related to $< K >$ by

$$H_c = p_c \frac{<K>}{J_s} \approx p_c \frac{K_1^4 D^6}{J_s A^3} \quad (1)$$

where p_c is dimensionless pre-factor of the order of unity, K_1 denotes the local magneto-crystalline anisotropy, J_s is the average saturation polarization and A is the exchange stiffness. The suppression of magneto-crystalline anisotropy requires that the randomly oriented grains are ferromagnetically coupled by exchange interaction. Consequently, if the exchange interaction is enhanced, the $< K >$ will be effectively averaged out and SMP will be improved [39,40]. It is interesting that the C_1 alloy possesses a lower D of 19 nm but it exhibits a larger H_c of 5.3 A/m compared with the C_2 alloy. This phenomenon can also be explained by the grain coupling effect as the V_{cry} is 50.4% for the C_1 alloy, which indicates a weaker exchange coupling between crystallites compared with that of the C_2 alloy. As for the frequency and *DC* superposition performance, it has been confirmed by the previous work that resistance to *DC* bias is related to the arrangement of magnetic domain structure [41]. The microstructure observation has suggested that the alloy with a higher C content exhibits comparatively larger magneto-crystalline anisotropy, which means the domain rearrangement is harder under applied field, therefore improves the resistance to applied *DC* field. The combination of high B_s and high resistance to *DC* bias promises potential material in high magnetic field amplitude and *DC* superposition application.

4. Conclusion

In conclusion, the influence of C substitution for P on amorphous forming ability, crystallization behavior, microstructure and soft magnetic properties in $Fe_{83.3}Si_4B_8P_{4-x}C_xCu_{0.7}$ alloy system was investigated. The results show that C substitution inhibits the precipitation of α-Fe phase in the quenching process. The formation of competing crystalline α-Fe phases with different textures is beneficial for the AFA. B_s increases with increasing C substitution due to the increase in V_{cry} of α-Fe nanocrystals, while excessive C addition leads to larger H_c but improves the resistance to applied *DC* field. The $Fe_{83.3}Si_4B_8P_2C_2Cu_{0.7}$ nanocrystalline alloy is developed with relatively higher AFA with 35 μm in critical thickness, high B_s of 1.84 T, low H_c of 4.8 A/m, high μ_e of 13,540, as well as better frequency characteristic and resistance to *DC* bias. The results can provide guidance for synthesizing novel soft magnetic materials with high AFA and good SMP.

Acknowledgments

This work was supported by the National Key Research and Development Program of China (Grant No. 2016YFB0300501), the National Natural Science Foundation of China (Grant Nos. 51631003, 51401052 and 51871237) and the Fundamental Research Funds for the Central Universities (Grant No. 2242018 K40112).

References

[1] Y. Yoshizawa, S. Oguma, K. Yamauchi, New Fe-based soft magnetic alloys composed of ultrafine grain structure, J. Appl. Phys. 64 (1988) 6044–6046.
[2] K. Suzuki, A. Makino, A. Inoue, T. Masumoto, Soft magnetic properties of nanocrystalline bcc Fe-Zr-B and Fe-M-B-Cu (M = transition metal) alloys with high saturation magnetization (invited), J. Appl. Phys. 70 (1991) 6232–6237.
[3] M.A. Willard, D.E. Laughlin, M.E. McHenry, Structure and magnetic properties of $(Fe_{0.5}Co_{0.5})_{88}Zr_7B_4Cu_1$ nanocrystalline alloys, J. Appl. Phys. 84 (1998) 6773–6777.
[4] M.E. McHenry, M.A. Willard, D.E. Laughlin, Amorphous and nanocrystalline materials for applications as soft magnets, Prog. Mater. Sci. 44 (1999) 291–433.
[5] J. Petzold, Applications of nanocrystalline soft magnetic materials for modern electronic devices, Scr. Mater. 48 (2003) 895–901.
[6] Y. Yoshizawa, M. Ohta, Magnetic properties of nanocrystalline Fe-Cu-Si-B alloys, J. Phys. Conf. Ser. 144 (2009) 120711.
[7] A. Makino, H. Men, K. Yubuta, T. Kubota, Soft magnetic FeSiBPCu hetero-amorphous alloys with high Fe content, J. Appl. Phys. 105 (2009) 013922.
[8] A. Makino, T. Kubota, K. Yubuta, A. Inoue, A. Urata, H. Matsumoto, S. Yoshida, Low core losses and magnetic properties of $Fe_{85-86}Si_{1-2}B_8P_4Cu_1$ nanocrystalline alloys with high B for power applications (invited), J. Appl. Phys. 109 (2011) 07A302.
[9] T. Bitoh, A. Makino, A. Inoue, A.L. Greer, Large bulk soft magnetic $((Fe_{0.5}Co_{0.5})_{0.75}B_{0.20}Si_{0.05})_{96}Nb_4$ glassy alloy prepared by B_2O_3 flux melting and water quenching, Appl. Phys. Lett. 88 (2006).
[10] C. Duhamel, K.G. Georgarakis, A. Lemoulec, A.R. Yavari, G. Vaughan, A. Baron, N. Lupu, Influence of fluxing in the preparation of bulk Fe-based glassy alloys, J. Alloys Compd. 483 (2009) 243–246.
[11] J. Pang, A.D. Wang, S.Q. Yue, F.Y. Kong, K.Q. Qiu, C.T. Chang, X.M. Wang, C.T. Liu, Fluxing purification and its effect on magnetic properties of high-Bs FeBPSiC amorphous alloy, J. Magn. Magn. Mater. 433 (2017) 35–41.
[12] Y. Zhang, P. Sharma, A. Makino, Effects of cobalt addition in nanocrystalline $Fe_{83.3}Si_4B_8P_4Cu_{0.7}$ soft magnetic alloy, IEEE Trans. Magn. 50 (2014) 2003004.

[13] A.D. Setyawan, K. Takenaka, P. Sharma, M. Nishijima, N. Nishiyama, A. Makino, Magnetic properties of 120-mm wide ribbons of high B_s and low core-loss NANOMET alloy, J. Appl. Phys. 117 (2015) 17B715.

[14] A.D. Wang, C.L. Zhao, A.N. He, H. Men, C.T. Chang, X.M. Wang, Composition design of high B_s Fe-based amorphous alloys with good amorphous-forming ability, J. Alloys Compd. 656 (2016) 729–734.

[15] K. Takenaka, A.D. Setyawan, P. Sharma, N. Nishiyama, A. Makino, Industrialization of nanocrystalline Fe-Si-B-P-Cu alloys for high magnetic flux density cores, J. Magn. Magn. Mater. 401((2016) 479–483.

[16] J. Xu, Y.Z. Yang, W. Li, X.C. Chen, The effect of introduction of carbon on the glass forming ability and magnetic properties of melt-spun Fe-Si-B-Cu-C alloys, J. Non-Cryst. Solids 447 (2016) 167–170.

[17] J. Xu, Y.Z. Yang, W. Li, Z.W. Xie, X.C. Chen, Effect of the substitution of C for Si on microstructure, magnetic properties and bending ductility in high Fe content FeSiBCuPC alloy ribbons, J. Alloys Compd. 727 (2017) 610–615.

[18] A. Makino, Nanocrystalline soft magnetic Fe-Si-B-P-Cu alloys with high B of 1.8-1.9 T contributable to energy saving, IEEE Trans. Magn. 48 (2012) 1331–1335.

[19] J. Xu, Y.Z. Yang, W. Li, X.C. Chen, Z.W. Xie, Effect of P addition on glass forming ability and soft magnetic properties of melt-spun FeSiBCuC alloy ribbons, J. Magn. Magn. Mater. 417((2016) 291–293.

[20] Y. Han, Z. Wang, Excellent high-temperature magnetic softness in a wide temperature for FeCo-based nanocrystalline alloy, J. Non-Cryst. Solids 434 (2016) 92–95.

[21] L. Xue, H.S. Liu, L.T. Dou, W.M. Yang, C.T. Chang, A. Inoue, X.M. Wang, R.W. Li, B.L. Shen, Soft magnetic properties and microstructure of $Fe_{84-x}Nb_2B_{14}Cu_x$ nanocrystalline alloys, Mater. Deign 56 (2014) 227–231.

[22] F.G. Chen, Y.G. Wang, Investigation of glass forming ability, thermal stability and soft magnetic properties of melt-spun $Fe_{83}P_{16-x}Si_xCu_1$ (x = 0, 1, 2, 3, 4, 5) alloy ribbons, J. Alloys Compd. 584 (2014) 377–380.

[23] E. Lopatina, I. Soldatov, V. Budinsky, M. Marsilius, L. Schultz, G. Herzer, R. Schäfer, Surface crystallization and magnetic properties of $Fe_{84.3}Cu_{0.7}Si_4B_8P_3$ soft magnetic ribbons, Acta Mater. 96 (2015) 10–17.

[24] R. Busch, W. Liu, L. Johnson, Thermodynamics and kinetics of the $Mg_{65}Cu_{25}Y_{10}$ bulk metallic glass forming liquid, J. Appl. Phys. 83 (1998) 4134–4141.

[25] L.M. Wang, Y.J. Tian, R.P. Liu, W.H. Wang, A "universal" criterion for metallic glass formation, Appl. Phys. Lett. 100 (2012) 261913.

[26] P. Gao, W.K. Tu, P.F. Li, L.M. Wang, Variation in entropies of fusion driven by mixing in binary glass forming eutectics, J. Alloys Compd. 736 (2018) 12–16.

[27] A. Takeuchi, A. Inoue, Classification of bulk metallic glasses by atomic size difference, heat of mixing and period of constituent elements and its application to characterization of the main alloying element, Mater. Trans. JIM 46 (2005) 2817–2829.

[28] Z.P. Lu, C.T. Liu, Role of minor alloying additions in formation of bulk metallic glasses: a Review, J. Mater. Sci. 39 (2004) 3965–3974.

[29] F.L. Kong, A.D. Wang, X.D. Fan, H. Men, B.L. Shen, G.Q. Xie, A. Makino, A. Inoue, High B_s $Fe_{84-x}Si_4B_8P_4Cu_x$ (x = 0-1.5) nanocrystalline alloys with excellent magnetic softness, J. Appl. Phys. 109 (2011) 07A303.

[30] M. Ohta, Y. Yoshizawa, Magnetic properties of nanocrystalline $Fe_{82.65}Cu_{1.35}Si_xB_{16-x}$ alloys (x = 0–7), Appl. Phys. Lett. 91 (2007) 062517.

[31] J. Füzerová, J. Füzer, P. Kollár, R. Bureš, M. Fáberová, Complex permeability and core loss of soft magnetic Fe-based nanocrystalline powder cores, J. Magn. Magn. Mater. 345 (2013) 77–81.

[32] T. Liu, F.Y. Kong, L. Xie, A.D. Wang, C.T. Chang, X.M. Wang, C.T. Liu, Fe(Co) SiBPCCu nanocrystalline alloys with high B_s above 1.83 T, J. Magn. Magn. Mater. 441 (2017) 174–179.

[33] P. Sharma, X. Zhang, Y. Zhang, A. Makino, Competition driven nanocrystallization in high B_s and low core loss Fe-Si-B-P-Cu soft magnetic alloys, Scr. Mater. 95 (2015) 3–6.

[34] K. Hono, D.H. Ping, M. Ohnuma, H. Onodera, Cu clustering and Si partitioning in the early crystallization stage of an $Fe_{73.5}Si_{13.5}B_9Nb_3Cu_1$ amorphous alloy, Acta Mater. 47 (1999) 997–1006.

[35] Y.H. Li, X.J Jia, Y.Q Xu, C.T Chang, G.Q. Xie, W. Zhang, Soft magnetic Fe-Si-B-Cu nanocrystalline alloys with high Cu concentrations, J. Alloys Compd. 722 (2017) 859–863.

[36] M. Matsuura, Y. Zhang, M. Nishijima, A. Makino, Role of P in nanocrystallization of $Fe_{85}Si_2B_8P_4Cu_1$, IEEE Trans. Magn. 50 (2014) 2003304.

[37] M. Nishijima, M. Matsuura, Y. Zhang, A. Makino, Observation of Cu nanometre scale clusters formed in $Fe_{85}Si_2B_8P_4Cu_1$ nanocrystalline soft magnetic alloy by a spherical aberration-corrected TEM/STEM, Philos. Mag. Lett. 95 (2015) 277–284.

[38] H.E. Kissinger, Reaction kinetics in differential thermal analysis, Anal. Chem. 29 (1957) 1702.

[39] G. Herzer, Grain size dependence of coercivity and permeability in nanocrystalline ferromagnets, IEEE Trans. Magn. 26 (1990) 1397–1402.

[40] G. Hezer, Modern soft magnets: amorphous and nanocrystalline materials, Acta Mater. 67 (2013) 718–734.

[41] X.D. Fan, M. Li, T. Zhang, C.C. Yuan, B.L. Shen, Effect of magnetic field annealing on soft magnetic properties of $Co_{71}Fe_2Si_{14-x}B_{9+x}Mn_4$ amorphous alloys with low permeability, AIP Adv. 8 (2018) 056105.